19th International Conference on
Adaptive Structures and Technologies
October 6-9, 2008
Ascona, Switzerland

A Study of the Transient Charging Behavior of Several Approaches to Piezoelectric Energy Harvesting

A. M. Wickenheiser[1]*, T. Reissman[1], E. Garcia[1], W. J. Wu[2]
[1] **Sibley School of Mechanical and Aerospace Engineering, Cornell University, Ithaca, New York, USA**
[2] **Department of Engineering Science and Ocean Engineering, National Taiwan University, Taipei**
*** Corresponding author: 138 Upson Hall, Ithaca, NY 14853**
Tel: 1 (607) 255-0710 Fax: 1 (607) 255-1222, E-mail: amw30@cornell.edu

ABSTRACT

This paper presents several designs for harvesting energy from a piezoelectric transducer to charge a storage capacitor. These designs involve the synchronized discharge or inversion of the voltage stored in the piezoelectric beam at the peak of its displacement. Specifically, the transient dynamics of the system during the charging phase are analyzed. These dynamics are important for low-voltage applications, such as wireless sensors, where the useable voltage across the storage unit is much lower than the open-circuit voltage of the piezeoceramic. Theoretical models of each harvesting circuit design are developed in order to predict the time-varying power delivered to the storage capacitor and the time required to charge it to a specified voltage. The differences in these theoretical circuits and physically realizable ones are presented. Also, an analysis of the errors introduced by modeling assumptions and non-ideal circuit components is given. These errors are cited in order to justify the deviations in experimental results from theoretical predictions.

Keywords: piezoelectric, power harvesting, charging dynamics

1. INTRODUCTION

Interest in extending the useable lifetime of wireless sensors and communications systems has generated much recent research in power harvesting systems. In particular, harvesting power from ambient vibrations using piezoelectric material is a promising means to gather energy from the environment (see [1] for a review). Recent research in the field of piezoelectric power harvesting has focused on improved modeling of the electromechanical transducer [2,3] and developing more sophisticated harvesting circuits than the typical rectifier [4,5].

In order to extend the range of applicability of power harvesting systems, the harvesting energy can be stored and used in bursts for devices requiring more power than is gathered. In such a system, an energy storage buffer is necessary to store the energy harvested temporarily when the device is idle and then release the energy when the device is turned on. Rechargeable batteries are an option for this energy storage purpose. Unfortunately, rechargeable batteries have notorious memory effects and have limited charge/discharge endurance; thus, field-deployed wireless sensors need to be serviced when the installed battery breaks down. Ultra-/super capacitors are another promising energy storage buffer. Unfortunately, the properties of ultra-capacitors are much different from those of rechargeable batteries: ultra-capacitors are characterized as reactive loads as opposed to resistive

loads and have several shortcomings, such as low sustained voltage and high leakage. Unlike rechargeable batteries, however, capacitors have high reusability and high repeatability in performance. Because of its reactive characteristic, the charging and interfacing circuit for an ultra-capacitor must be designed differently from one for a rechargeable battery. Indeed, understanding the dynamics of energy storage is critical to developing a system that maximizes the duty cycle of the load.

In this paper, the power output from energy harvesting sources to storage devices is investigated for several circuit designs. Specifically, a direct charging methodology and a synchronous charge extraction technique are utilized. With the latter technique, the energy taken out from the piezoelectric transducer is quadrupled over the matching resistive load case. The major concern of this study, however, is how this increased energy can be completely transferred into a large storage capacitor. The differences between a simple resistive and capacitive load and the synchronized switching circuit for pure capacitive loads are detailed. The transient power delivered to the storage capacitor and the charging curves for several techniques are presented. Finally, these theoretical results are compared with experimental data and discussed.

2. THEORETICAL MODELING

2-1. Piezoelectric transducer model

The schematic and equivalent circuit diagram of a cantilevered piezoelectric transducer generally used in vibration energy harvesting is shown in figure 1. The governing equation of the model can be derived from the beam dynamics equation and Kirchhoff's Current Law, and are written as

$$M\ddot{u} + \eta_m \dot{u} + Ku + \Theta V_p = F(t), \tag{1}$$

$$-\Theta \dot{u} + C_0 \dot{V}_p = -I(t), \tag{2}$$

where M is the mass of the beam, η_m is the mechanical damping coefficient of the beam, K is the effective stiffness of the structure, u is displacement of the beam tip, F is the applied external force, Θ is the equivalent piezoelectric constant (forcing factor), V_p is the terminal voltage of the piezoelectric transducer, I is the output current from piezoelectric transducer, and C_0 is its clamped (i.e. no strain) intrinsic capacitance [6,7]. The model given by Equations (1-2) assumes that only one mode of vibration is excited in the system, whether by the external force or the influence of the electrical system. Thus, only one position coordinate is necessary to describe the motion of the beam, and it is chosen to be the displacement of the beam tip.

In order to convert this electromechanical system into a purely electrical one for analysis, the coupling term $\Theta\dot{u}$ can be modeled as a current source, I_P. Assuming that the motion of the beam is sinusoidal with amplitude u_0 and natural frequency ω, the piezoelectric transducer equivalent current source can be represented as

$$I_P(t) = \Theta\dot{u} = \Theta u_0 \omega \sin(\omega t) = \hat{I}_P \sin(\omega t), \tag{3}$$

where $\hat{I}_P$ is the amplitude of the equivalent current source.

Throughout the forthcoming mathematical analysis, it is assumed that the coupling between the mechanics and the electronics in the system is negligible. This is equivalent to assuming that the electrical energy removed from the transducer during each cycle is small compared to the vibrational

energy imparted to the beam through base excitation. This simplification permits the assumption of a constant beam tip deflection during the entire power harvesting process.

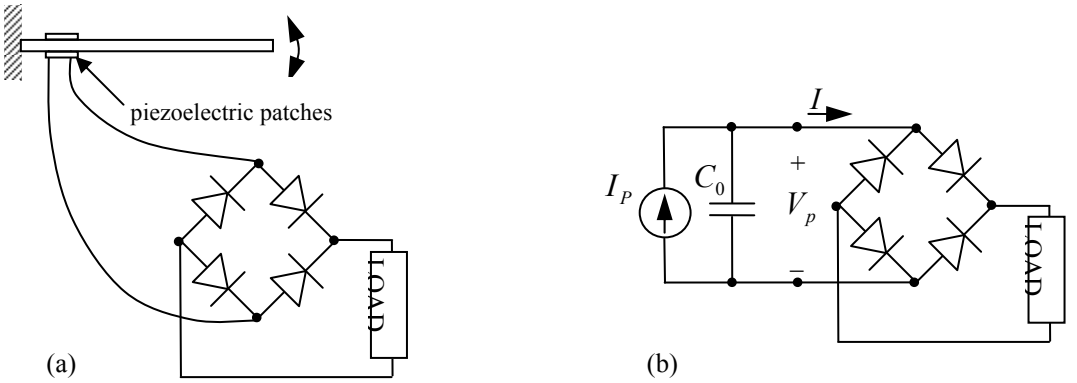

Figure 1. (a) Schematic diagram of a cantilever configuration piezoelectric transducer energy harvester. (b) The equivalent circuit diagram of this configuration.

2-2. Optimal resistive load

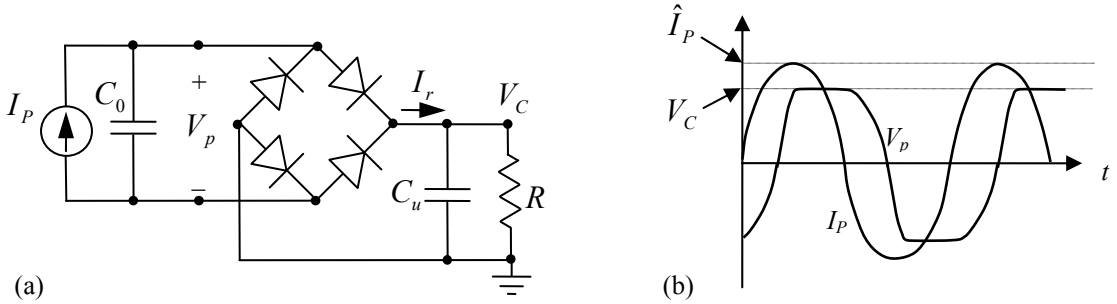

Figure 2. (a) Schematic diagram of the piezoelectric transducer with a resistive load after a full wave bridge rectifier. (b) Steady-state source current and output voltage waveforms.

Before analyzing the charging of a large external storage capacitor, the resistive load case is first presented as a reference case for the pure capacitive load cases to follow. This case is often cited as the "standard interface" in much of the piezoelectric power harvesting literature [6,7]. Figure 2(a) shows the schematic diagram of the piezoelectric transducer with a resistive load after a full wave bridge rectifier, and figure 2(b) shows the steady state waveforms of the beam displacement and the voltage across the resistor V_c. Integrating (2) over a half-cycle yields the terminal voltage of the load resistor given by

$$V_C = \frac{2R\Theta\omega u_0}{2RC_0\omega + \pi} \equiv \frac{2R\hat{I}_P}{2RC_0\omega + \pi}. \tag{4}$$

The output power of generator is then

$$P = \frac{V_C^2}{R} = \frac{4R\Theta^2\omega^2 u_0^{\,2}}{(2RC_0\omega + \pi)^2} \equiv \frac{4R\hat{I}_P^{\,2}}{(2RC_0\omega + \pi)^2}. \tag{5}$$

The output power given by (5) can be maximized by varying the load resistance R, yielding

$$R_{\text{opt}} = \frac{\pi}{2C_0\omega} \quad \text{, and} \quad P_{\max} = \frac{\Theta^2\omega u_0^{\,2}}{2\pi C_0} = \frac{\hat{I}_P^{\,2}}{2\pi\omega C_0}. \tag{6}$$

This maximum power, obtained by optimizing the load resistance, is the baseline value of output power referenced in the subsequent sections.

2-3. Direct charging of a storage capacitor

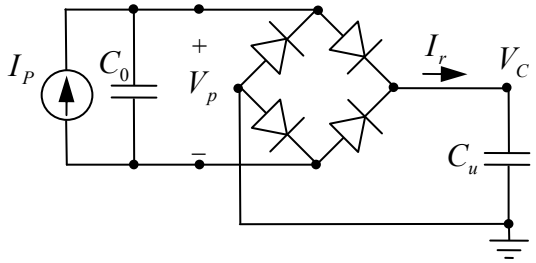

Figure 3. Schematic diagram of a storage capacitor loading after a full wave rectifier.

Figure 3 shows the schematic of a storage capacitor loading after the full wave rectifier. As the voltage across the piezoelectric increases due to the bending of the beam, the diodes in the rectifier begin conducting, and both the internal and external capacitors are henceforth charged simultaneously. As the charging process progresses, the phase during the cycle at which the diodes begin conducting approaches the start of the next half-cycle. Therefore, the charge passing through the diodes during each half-cycle decreases, thereby reducing the increase in the external capacitor voltage per cycle.

The analysis presented in [8] shows that the voltage across the storage capacitor V_C can be found recursively as

$$V_{C,i+1} = V_{C,i}\left(1 - \frac{2C_0}{C_u + C_0}\right) + \frac{2\hat{I}_P}{\omega(C_u + C_0)}. \tag{7}$$

This equation can be written explicitly in the form of a geometric series:

$$V_{C,i} = \sum_{n=0}^{i-1} A^n B = \frac{B(A^i - 1)}{A - 1} \quad \text{, for } i \geq 1, \text{where } A = 1 - \frac{2C_0}{C_u + C_0} = \frac{C_u - C_0}{C_u + C_0};\ B = \frac{2\hat{I}_P}{\omega(C_u + C_0)}. \tag{8}$$

As i approaches infinity, the voltage of the external storage capacitor approaches a steady-state value of

$$V_{C,\infty} \equiv \lim_{i\to\infty}\left(\sum_{n=0}^{i-1} A^n B\right) = \frac{B}{1 - A} = \frac{\hat{I}_P}{\omega C_0} = \hat{V}_{OC}, \tag{9}$$

and the stored energy approaches $\frac{1}{2}\left(C_u \hat{V}_{OC}^2\right)$. At this point, the diodes are never conducting, and no energy is transferred to the storage capacitor.

The average power charging the storage capacitor in the i^{th} half-cycle $\overline{P}_i, (i \geq 1)$ can be obtained by the stored energy increase in the half-cycle divided by the half-cycle period, $T/2$.

$$\overline{P}_i = \frac{\frac{1}{2}C_u(V_{C,i}^2 - V_{C,i-1}^2)}{T/2} = \frac{\omega C_u}{2\pi}\left\{\left[\left(\frac{C_u - C_0}{C_u + C_0}\right)^2 - 1\right]V_{C,i-1}^2 + \frac{4\hat{I}_P C_0(C_u - C_0)}{\omega(C_u + C_0)^2}V_{C,i-1} + \frac{4\hat{I}_P^2}{\omega^2(C_u + C_0)^2}\right\}. \tag{10}$$

Equation (10) shows that the power delivered from the piezoelectric transducer charging the external storage capacitor is zero in the beginning of charging process, reaches its maximum when the storage capacitor voltage is half of the open-circuit voltage, and then falls back to zero as the charging voltage reaches the final voltage, i.e. the open circuit voltage amplitude. The peak value of the average power delivered during a half cycle in the capacitive load charging process is equal to the maximum power with an optimal resistive load. Thus, charging a pure capacitive load is equivalent to charging a time-varying resistive load. At the beginning of the charging process, the terminal voltage and the charging power are zero; this state is equivalent to short circuit condition or a zero-value resistive load. When the storage capacitor is charged to half the open circuit voltage amplitude, the charging power reaches maximum, and this state is equivalent to an optimal (or matched) resistor load. At the end of charging process, the final voltage approaches the open-circuit voltage amplitude, and the charging current and power decrease to zero. This state is equivalent to an infinite-value resistive load.

2-4. Synchronized Switching and Discharging to a storage Capacitor (SSDC)

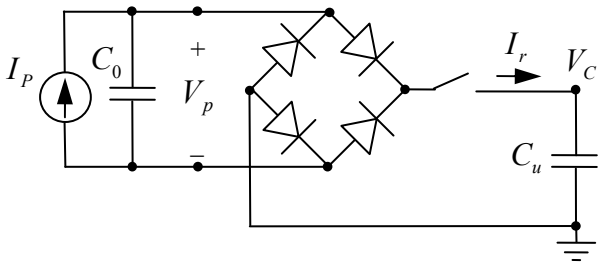

Figure 4. Schematic diagram of the SSDC case.

In this scenario, a switch is inserted before the external storage capacitor, but the circuit is otherwise the same as the previous case. This switch is only closed for a short interval when the displacement reaches its peak or the equivalent current source waveform crosses zero. Thus, in this circuit the storage capacitor is charged instantaneously at the end of each half-cycle by the energy stored in the piezoelectric capacitance instead of continuously during the cycle. Figure 4 shows the circuit diagram of the SSDC case. When the switch is open, the piezoelectric transducer is in open circuit, and the current is charging the piezoelectric capacitor C_0. When the equivalent current source waveform crosses zero, the switch is closed to discharge the energy stored in C_0 into the storage capacitor C_u. Since there is no impedance between the capacitors, the discharge is completed in infinitesimal time.

While the switch is open, the transducer vibrates from peak to peak, and so the voltage across the piezoelectric capacitor V_p swings through $2\hat{V}_{OC}$. Thus, the voltage across the piezoelectric before the i^{th} discharge is given by

$$|V_{p,i}| + V_{C,i-1} = 2\hat{V}_{OC} = \frac{2\hat{I}_p}{\omega C_o}, \tag{11}$$

where, $V_{C,i-1}$ is the storage capacitor voltage at the beginning of the i^{th} half-cycle of vibration, and $V_{C,0}$=0. The storage capacitor voltage at the beginning of the next half-cycle, $V_{C,i}$, can be obtained by considering a charge re-balance during the infinitesimal discharge interval, under the assumptions of no charge loss and that the charge supplied by the transducer is zero during this interval. This conservation of charge yields

$$Q_{total} = C_0 |V_{p,i}| + C_u V_{C,i-1} = (C_0 + C_u) V_{C,i}. \tag{12}$$

By substituting (11) into (12), the relationship between $V_{C,i}$ and $V_{C,i-1}$ can be obtained as

$$V_{C,i} = \frac{C_u - C_0}{C_u + C_0} V_{C,i-1} + \frac{2\hat{I}_P}{\omega(C_u + C_0)}. \tag{13}$$

This equation can be rewritten explicitly as

$$V_{C,i} = \sum_{n=0}^{i-1} C^n D = \frac{D(C^i - 1)}{C - 1} \quad \text{, for } i \geq 1 \text{ and } C = \frac{C_u - C_0}{C_u + C_0};\ D = \frac{2\hat{I}_P}{\omega(C_u + C_0)} \tag{14}$$

In comparison to the previous case of direct charging, $C=A$ and $D=B$, and so the charging process in the SSDC case is completely the same as the previous case.

The average power output from the piezoelectric transducer in the i^{th} half-cycle is equal to the power charging its internal capacitance in the half-cycle, given by

$$\overline{P_i} = \frac{\frac{1}{2} C_0 (V_{p,i}^2 - V_{C,i-1}^2)}{T/2} = \frac{2}{\pi}\left(\frac{\hat{I}_P{}^2}{C_0 \omega} - \hat{I}_P V_{C,i-1} \right). \tag{15}$$

Equation (15) indicates that at the beginning of the charging process the power charging the internal static capacitor is 4 times the maximum power with the optimal resistive load and linearly decreases to zero by the end of charging process. However, the power charging the external capacitor is completely the same as the previous direct charging case. At the instance of discharge, the piezoelectric transducer terminal voltage drops from $|V_{p,i}|$ to $V_{C,i}$ in infinitesimal time, and, consequently, the loss in potential energy is

$$\Delta E = \frac{1}{2} C_0 V_{p,i}^2 + \frac{1}{2} C_u V_{C,i-1}^2 - \frac{1}{2}(C_0 + C_u) V_{C,i}^2 = \frac{2 C_0 C_u}{C_0 + C_u}\left(V_{C,i-1} - \hat{V}_{OC} \right)^2. \tag{16}$$

This energy loss is greatest at the beginning of the charging process, when $V_{C,i}$ is small, and decreases to 0 as $V_{C,i}$ approaches $\hat{V}_{OC}$. Since there are no assumed losses in this system, this energy is converted back into the kinetic energy of the beam. Thus, although the SSDC case increases the power output from the piezoelectric transducer by discharging the piezoelectric at the peaks of the vibration, the extra energy is lost again in the infinitesimal discharge interval when charging the external storage capacitor.

2-5 Synchronized Switching and Discharging to a storage Capacitor through an Inductor (SSDCI)

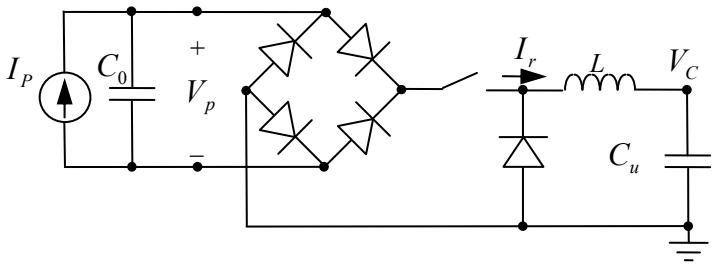

Figure 5. Schematic diagram of the SSDCI case.

In order to gain back the lost energy during the discharge interval in the previous SSDC case, an inductor in inserted before the storage capacitor. As the piezoelectric capacitor discharges, energy is stored in the inductor, which continues to charge the storage capacitor even after the voltage across the piezoelectric drops to 0. The circuit diagram of the SSDCI case is shown in figure 5. Once again, the switch is open during the majority of the vibration cycle, the piezoelectric transducer is in open circuit, and the equivalent current source is charging the piezoelectric capacitor C_0. As in the SSDC case, when the vibration reaches its peak, the switch is closed to discharge the energy stored in C_0 into the storage capacitor C_u. With the series inductor inserted, the discharging time is not infinitesimal but dictated by the LC resonance cycle time.

The analysis detailed in [8] gives the expression for $V_{C,i+1}$ for the general case of a lossy inductor. If a lossless circuit is considered, however, $V_{C,i+1}$ can be expressed simply as

$$V_{C,i+1} = \sqrt{\frac{C_0}{C_u} V_{p,i}^{\ 2} + V_{C,i}^{\ 2}} \quad \text{, which implies } V_{C,i} = \sqrt{i \frac{C_0}{C_u}} \, | V_{p,i} | . \tag{17}$$

During the initial stage of the charging process, when C_0 discharges all the way to 0, $\left| V_{p,i} \right| = 2\hat{V}_{OC}$. Thus, in the lossless case,

$$V_{C,i} = 2\hat{V}_{OC} \sqrt{i \frac{C_0}{C_u}} . \tag{18}$$

The average power in i^{th} half-cycle is then

$$\overline{P_i} = \frac{\frac{1}{2} C_u (V_{C,i+1}^{\ 2} - V_{C,i}^{\ 2})}{T/2} = \frac{2\hat{I}_P^{\ 2}}{C_0 \omega \pi} = 4P_{\max} . \tag{19}$$

Equation (19) indicates that, in the lossless case, the average power for each cycle is 4 times the maximum power with the optimal resistive load during the time when C_0 still discharges all the way to 0. This result is reflected in the findings of [5], who showed that the harvested power for the SSDCI case is independent of the applied resistive load.

The final charging voltage and the $V_{C,i}$ with finite quality factor are both difficult to solve analytically. However, the charging curve and final charging voltage can be simulated numerically. These simulations are plotted in figure 6 for various values of inductor quality factor Q_I.

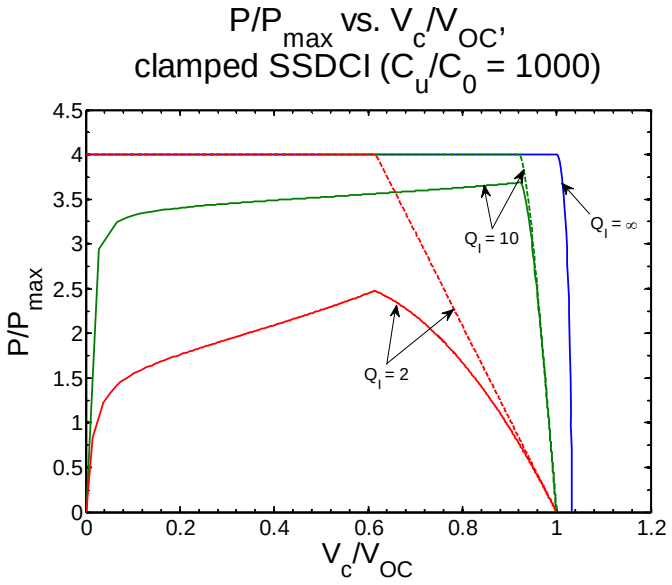

Figure 6. Charging power versus voltage for the internal piezoelectric capacitance C_0 (dashed) and the storage capacitor C_u (solid) for Q_I = 2,10,∞.

For the case of $Q_I = \infty$, the charging power is four times the matched resistive power until $V_{C,i}$ approaches the open-circuit voltage. Once $V_{C,i}$ increases past this point, the charging power drops off quickly due to the large ratio of storage to piezoelectric capacitance. As Q_I decreases, this threshold voltage decreases. Also, the average and peak charging powers decrease as more energy is consumed by the resistance of the inductor. This is especially true near the beginning of the charging process when the current through the inductor is greatest. However, even with a low quality factor of 2, the charging power is significantly greater than the maximum charging power of the previous two cases for most of the charging process.

3. EXPERIMENTAL VALIDATION

The main components of the experimental setup used in this study are depicted in figure 7. The electromechanical transducer is composed of a uniaxially oscillating cantilever beam with piezoelectric patches bonded 2mm from the clamped end to form a parallel bimorph configuration. The piezoelectric patches are PSI-5A4E ceramic with nickel plated electrodes from Piezo Systems, Inc., and the bonding adhesive is Loctite E-120HP Hysol epoxy from Henkel AG & Co. The piezoelectric patches are oriented with their lengths in the same direction as the beam length in a single row of 8 patches on the top surface and 8 patches on the bottom. The poling direction is orthogonal to the plane of the beam and is in the same direction for both rows, creating the parallel bimorph configuration. Thus, the piezoelectric response is dominant in the 31 direction. The piezoelectric patches are connected in parallel to the electronic circuitry. The beam is driven by a Bruel and Kjaer vibration exciter Type 4809, which has a first axial resonance frequency of 20kHz, well above the driving frequencies considered in this study. The beam material is cold-rolled annealed 1095 spring steel. The dimensions of the beam and the piezoelectric patches are given in table 1. The circuit diagram of the SSDCI experiment is shown in figure 7. An N-channel MOSFET, IRFU201, is used as the switch. Because the source terminal voltage rises as the storage capacitor C_u charges up, the pulsing control signal is AC-coupled through a photocoupler (a Sharp PC957L, not shown in the diagram) to the gate terminal. The gate resistor, (R_g =10Ω) is used to speed up the switch opening/closing time by charging/discharging the gate capacitance of the MOSFET. Another Schottky diode (D_b) between the switch and the inductor is used to block the reverse current and recover energy wasted in the oscillation. For the SSDC case, the circuit is the same as in figure 7 except that the inductor is not used, and the source terminal of the MOSFET is connected directly to the storage capacitor C_u.

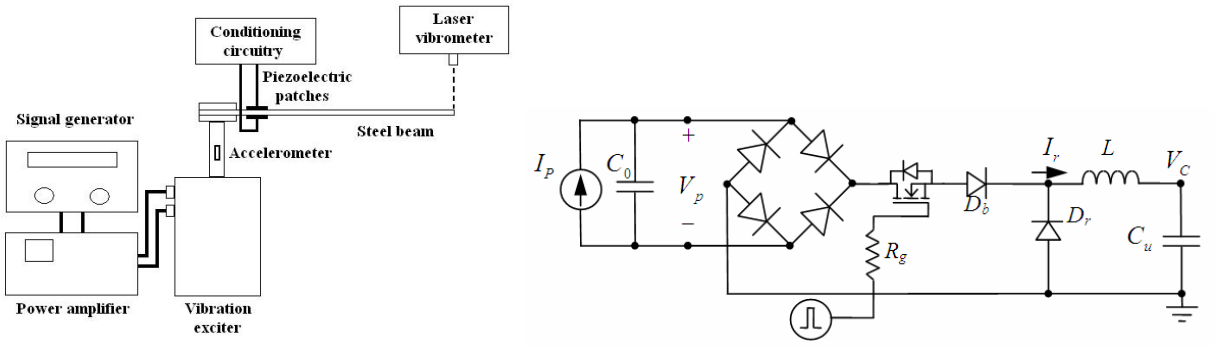

Figure 7. Experimental setup (left), Experimental SSDCI circuit (right)

Table 1. Dimensions of electromechanical transducer.

Steel Beam	182 x 95 x 1.825 [mm]
Piezoelectric Patch	15 x 5 x 0.508 [mm]

Measurements of the parallel bimorph's response are taken using an accelerometer at the drive output of the vibration exciter for measuring the base excitation, a laser vibrometer proximity sensor for measuring the beam tip deflection, and an Agilent, Inc. DSO-6104A oscilloscope for measuring the bimorph voltage and the voltage at several points in the electronic circuit. An HP4194A impedance analyzer is used to characterize the capacitors and inductor at the frequency of use, determined by the LC resonance frequency. Since there are losses associated with each of the components in the circuit, an overall effective quality factor Q_I is measured experimentally. The measured experimental parameters are listed in table 2. The electromechanical system parameters [the coefficients of Equations (1-2)] are estimated using the model identification procedure of [5].

Table 2. Experimental parameters.

f_0	short-circuit resonance frequency	65.38 [Hz]
f_1	open-circuit resonance frequency	65.46 [Hz]
C_0	net clamped capacitance of the piezoelectric elements	33.17 [nF]
Θ	equivalent piezoelectric constant	0.0018 [N/V]
η_m	equivalent damping coefficient	0.032 [N/(m/s)]
K	equivalent stiffness	40,800 [N/m]
M	mass	0.242 [kg]
C_u	storage capacitance	906.2 [nF] 1.795 [µF] 4.121 [µF] 8.301 [µF] 17.63 [µF] 25.85 [µF]
L	inductance	2.214 [mH]
Q_I	effective quality factor (SSDCI case)	2.6

Each of the three circuit topologies discussed above – direct charging, SSDC, and SSDCI – are tested experimentally with varying storage capacitors as listed in table 2. The experiment results are compared with the theoretical predictions and plotted in figure 8. Figure 8(a) shows the storage capacitor charging curves for the three cases with the largest storage capacitance (25.85 µF), which is 779.349 times C_0. All three cases match the trends of the theoretical predictions reasonably well. For the SSDC and SSDCI cases, there is an extra diode drop in the circuit so that the final voltage is less than that of the direct charging case. The SSDC case theoretically has the same performance as the direct charging case; however, there are losses associated with the switching that are not accounted for in the model. The charge accumulated in each half-cycle is discharged to the storage capacitor in a very short time, causing a high current through the switch and a loss due

to the resistance of the switch. Figure 8 also indicates that the charging speed of the SSDCI case is more than twice as fast as the other two cases.

Figure 8(b) shows the normalized piezoelectric transducer output power versus the terminal voltage of the storage capacitor. Both the direct charging and SSDC cases are fairly symmetric about 0.50 V_{OC}, as predicted. Their average efficiency, in terms of power, is around 80% and 65%, respectively, as shown in figure 8(b). The additional losses in the SSDC case are likely due to the switching, as discussed above. For the SSDCI case, the normalized output power rises to around 2 very quickly and slowly increases until the threshold voltage before falling back to zero, matching the trends of the predicted response. However, the experimental data for the output power are less than theoretically predicted. The major reason is most likely the switching losses when it turns on and off, which are not included in the experimental quality factor measurement described above. Nevertheless, despite these losses, the charging power is still at least 2 times larger than the direct charging case.

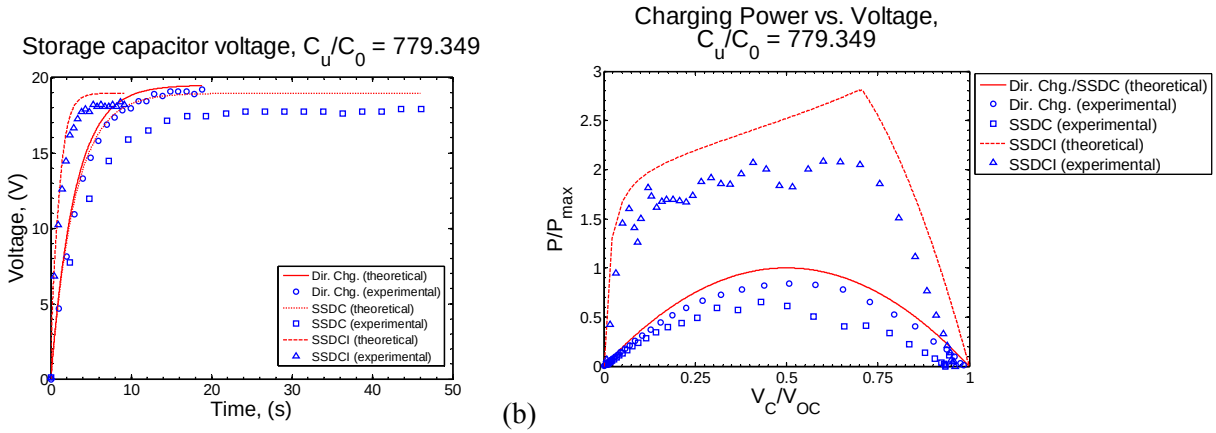

Figure 8. (a) Capacitor charging voltage versus time, (b)

4. CONCLUSIONS

In this paper, the transient charging behavior of a capacitive load for piezoelectric energy harvesting devices is modeled in depth for several circuit topologies. These cases are compared to the standard interface consisting of a matched resistive load after the rectifier. Directly charging a capacitor produces a similar power curve to a varying resistive load, and the experimental results match this trend with a conversion efficiency of 80%. In order to improve upon this method, two synchronous switching methods are considered, which are shown to charge the piezoelectric capacitance with up to 4 times the output power of the direct charging case. For the SSDC case, most of this boosted power is lost again in the potential drop during the infinitesimal discharge interval. The theoretical model indicates that this method has the same charging performance as direct charging; however, experimentally the losses due to the high discharge current lead to even poorer charging performance than direct charging. For the SSDCI case, an inductor is inserted in the path of the discharge, and the potential energy loss can be fully recovered in the ideal case of no losses. In real applications, though, the losses on the inductor and switch will degrade the boosted power and can be accurately modeled as a quality factor of the circuit. A circuit quality factor of 2.6 is demonstrated experimentally in this paper, and it is measured to have a charging power around 2 times the adaptive resistive load and has a much faster charging rate.

ACKNOWLEDGEMENTS

The authors would like to thank the National Science Council of Taiwan for the financial support of the scholar foreign visiting program under contract no. NSC 96-2918-I-002-031. They would also like to acknowledge the DCI Post-doc program and adviser Dr. Jim Beckwith for supporting this research. Additional support was provided from the DARPA Microsystems Technology Office HiMEMS Program through the Boyce Thompson Institute for Plant Research under the supervision of Dr. Amit Lal.

REFERENCES

1. Sodano, H. A., D. J. Inman, and G. Park, "A Review of Power Harvesting from Vibration using Piezoelectric Materials," *The Shock and Vibration Digest*, Vol. 36, No. 3, pp. 197-205 (May 2004).
2. Sodano, H. A., G. Park, and D. J. Inman, "Estimation of Electrical Charge Output for Piezoelectric Energy Harvesting," *Strain*, Vol. 40, pp. 49-58 (2004).
3. Erturk, A. and D. J. Inman, "A Distributed Parameter Electromechanical Model for Cantilevered Piezoelectric Energy Harvesters," *Journal of Vibration and Acoustics*, Vol. 130, 041002 (August 2008).
4. Ottman, G. K., H. F. Hofmann, and G. A. Lesieutre, "Optimized Piezoelectric Energy Harvesting Circuit Using Step-Down Converter in Discontinuous Conduction Mode," *IEEE Transactions on Power Electronics*, Vol. 18, No. 2, pp. 696-703 (March 2003).
5. Lefeuvre, E., A. Badel, C. Richard, and D. Guyomar, "Piezoelectric Energy Harvesting Device Optimization by Synchronous Electric Charge Extraction," *Journal of Intelligent Material Systems and Structures*, Vol. 16, pp. 863-876 (October 2005).
6. Guyomar D, A. Badel, E. Lefeuvre, and C. Richard, C, "Toward Energy Harvesting Using Active Materials and Conversion Improvement by Nonlinear Processing," *IEEE Trans. Ultrason. Ferroelectr. Freq. Control*, Vol. 52, pp. 584–595 (April 2005).
7. Shu Y. C., I. C. Lien, and W. J. Wu, "An improved analysis of the SSHI interface in piezoelectric energy harvesting," *Smart Mater. and Struct.* Vol. 16, pp. 2253–2264 (2007).
8. Wu, W. J., A. M. Wickenheiser, T. Reissman, and E. Garcia, "Modeling and experimental verification of synchronized discharging techniques for boosting power harvesting from piezoelectric transducers," *Smart Mater. and Struct.* (submitted).